THE JOURNAL OF PHYSICAL CHEMISTRY B

Article

pubs.acs.org/JPCB

Binding of Hydrogen-Citrate to Photoactive Yellow Protein Is Affected by the Structural Changes Related to Signaling State Formation

Marijke Hospes,[†] Johannes H. Ippel,[‡] Rolf Boelens,[‡] Klaas J. Hellingwerf,*[,†] and Johnny Hendriks[†]

[†]Laboratory for Microbiology, Swammerdam Institute for Life Sciences and Netherlands Institute for Systems Biology, Amsterdam, The Netherlands

[‡]Bijvoet Center for Biomolecular Research, Science Faculty, Utrecht University, Padualaan 8, 3584 CH, Utrecht, The Netherlands

Supporting Information

ABSTRACT: The tricarboxylic acid citric acid is a key intermediary metabolite in organisms from all domains of the tree of life. Surprisingly, this metabolite specifically interacts with the light-induced signaling state of the photoactive yellow protein (PYP), such that, at 30 mM, it retards recovery of this state to the stable ground state of the protein with up to 30%, in the range from pH 4.5 to pH 7. We have performed a detailed UV/vis spectroscopic study of the recovery of the signaling state of wild type (WT) PYP and two mutants, H108F and Δ25-PYP, derived from this protein, as a function of pH and the concentration of citric acid. This revealed that it is the dianionic form of citric acid that binds to the pB state of PYP. Its binding site is located in between the N-terminal cap and central β-sheet of PYP, which is accessible only in the signaling state of the protein. The obtained results show how changes in the distribution of subspecies of the signaling state of PYP influence the rate of ground state recovery.

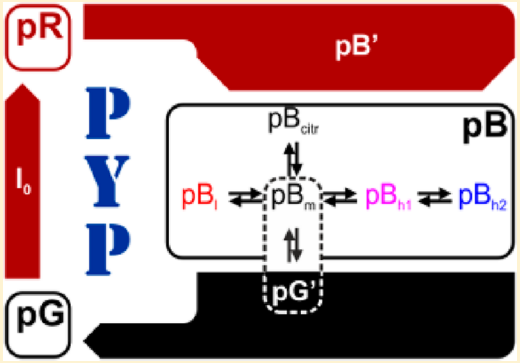

INTRODUCTION

Photoactive yellow protein (PYP) from *Halorhodospira halophila* is a relatively small (125 amino acids), water-soluble photoreceptor protein. For more than 10 years already, PYP has been studied intensely as a model system in photoreceptor research because (i) it is chemically and photochemically very stable,[1,2] (ii) shows considerable structural change during signaling state formation,[3] and (iii) it is the proto-type of the Per-Arnt-Sim (PAS) domain superfamily of signal transduction domains.[4] Most of these PAS domains are involved in protein−protein interactions and function as sensors and signal transducers.[5] For signal transfer, many bind, or interact with, a ligand or chromophore. PYP contains *p*-coumaric acid as a chromophore that is bound to the protein via a thiolester bond with C69.[6−8]

As a photoreceptor, PYP has a light induced photocycle. In this cycle, three major intermediates can be identified: pG, pR, and pB. In the ground state of PYP, pG (also named P or PYP), the chromophore is deprotonated and has a *trans* configuration.[9] The absorption maximum of pG is at 446 nm.[10] Upon excitation with light, the pR intermediate (also named I_1 or PYP_L) can be formed. Here the chromophore has received a *cis* configuration but is still deprotonated.[11] As a result, the absorption maximum (~460 nm) is red-shifted. The isomerization of the chromophore facilitates the formation of the signaling state pB (also named I_2, I_2', or PYP_M), where the chromophore is typically protonated and where the structure of the protein has changed significantly, compared to pG.[3,12] Furthermore, the absorption maximum is blue-shifted relative to pG. Presumably the structural changes that accompany pB formation lead to alteration of the interaction with a downstream, and currently poorly characterized, transducer.[13] pB subsequently recovers to pG, closing the photocycle.

Note that, depending on the conditions, certain characteristics of these basic phototcycle species may change. As such, we can divide these photocycle species into several subspecies. Depending on the conditions, one or more of these subspecies may then be dominantly present.[14] A prime example is the pB species. The light-induced structural changes in PYP show pronounced pH dependence, such that at low pH the amount of structural change is decreased[15] compared to neutral and moderately alkaline pH. The two corresponding subspecies of pB also display different absorption spectra, with the less unfolded form (i.e., the low-pH form of pB) having an absorption maximum of 368 nm and the more unfolded form having an absorption maximum of 355 nm.[14,16−18] At very high pH, a third form of pB can be formed, in which the solvent-exposed chromophore is deprotonated. This leads to a shift of the absorption maximum of pB to 430 nm.[14] Therefore, depending on the pH, one or more of these subspecies may be present in significant amounts.

Recently, a photocycle intermediate (pG′) was identified that appears to be important for speedy recovery from pB to pG.[14]

Received: July 11, 2012
Revised: October 15, 2012
Published: October 18, 2012

Recovery includes reisomerization of the chromophore and refolding of the protein.[14] The pG′ intermediate is characterized by a deprotonated chromophore in combination with a specific fold of the apoprotein. The intermediates pB and pG′ are in a fast pH-independent equilibrium, while the decay of pG′ to pG is pH-dependent. Recovery via pG′ is much faster than the direct recovery of pG from pB.[14]

The photocycle of PYP has been well-studied over the entire time-domain that is relevant for its functioning, i.e., from femtoseconds to seconds. In this study, we focus on the recovery reaction of the signaling state (pB) back to the ground state (pG). Solvent conditions, such as ionic strength,[17] temperature,[3] pH,[18,19] and buffer composition,[20] have an effect on the rate of this recovery. For example, the recovery rate decreases as the ionic strength is increased.[17] For this study, we have specifically studied the influence of citric acid, as it has been shown that, on top of its effect on ionic strength, it slows down the recovery rate of PYP more than other organic acids do.[20] As such, it may interact with potential signal transducer interaction sites. To resolve the specific site(s) of interaction between PYP and anionic species of citric acid, we have measured the pG recovery of WT PYP, and the mutants H108F and Δ25-PYP, as a function of both pH and citrate concentration, keeping temperature and ionic strength constant. From these measurements, we were able to determine that it is the dianionic form of citric acid that affects the recovery rate in WT PYP. In addition, for the mutant PYPs, we observed differences in the influence that citrate has on recovery. From these observations, we were able to deduce that the citrate-binding surface of PYP is located in between the N-terminal cap and the β-sheet. Subsequent NMR measurements support the assignment of this binding site for citrate.

MATERIALS AND METHODS

Preparation of Photoactive Yellow Protein. WT, H108F, and Δ25-PYP were produced and isolated as described previously for WT PYP.[21] Apo-PYP was reconstituted with the 1,1′-carbonyldiimidazole derivative of *p*-coumaric acid, as described in ref 22. For details on the purification of the proteins, see the Supporting Information. The purified holo-proteins were used without removal of the genetically introduced N-terminal hexa-histidine containing tag. Their purity index (OD_{280}/OD_{446}) was better than 0.5. A part of the samples were prepared with uniform ^{15}N labeling of PYP.[23]

Sample/Buffer Preparation. Buffer solutions with defined ionic strength were prepared by mixing 1 M acetic acid, 0.2 M Na_2HPO_4, 1 M Trizma base, 0.5 M boric acid, 4 M NaCl, 1 M HCl, and 1 M NaOH. The required amount of these stock solutions was calculated.[14] Where necessary, minor pH adjustments were made with either 1 M HCl or NaOH.

Transient ms/s UV/vis Spectroscopy. UV/vis spectra were recorded using an HP8453 UV/vis spectrophotometer. Time resolved spectra were recorded from 250 to 600 nm, using an integration time of 0.1 s. A "Kraayenhof" cuvette[24] was used to thermostat the sample at 25 °C, and allowed measurement of the sample pH in the measurement setup. A Schott KL1500 LCD lamp was used to illuminate the sample. Actual sample illumination was computer controlled via a shutter system, allowing synchronization of sample illumination with the spectroscopic measurement. A 2 s delay was used between the start of the measurement and a typical 5 s illumination period of the sample.

Data Analysis: Transient UV/vis Data. Data sets obtained for each condition were analyzed as described previously.[14] From this analysis, both recovery rate constants and pB spectra were extracted. A typical analysis is described in the Supporting Information.

Data Analysis: Spectral. The pH and citrate-concentration dependence of the pB spectra obtained from the transient UV/vis data was analyzed using the model depicted inside the "pB balloon" in Figure 2. The rationale behind this model is further explained in the Results section. Equation 1 is a mathematical description of the fraction of each species in this model as a function of pH and citrate concentration. Here the subscripts A–E represent the different pB species: A, pB_l; B, pB_m/pG′ mixture; C, pB_{h1}; D, pB_{h2}; E, pB_{citr}. K_{citr} represents the binding constant of $HCitrate^{2-}$ to pB_m (for a detailed explanation of this nomenclature, see the caption of Figure 2). Note that $[HCitrate^{2-}]$ is pH dependent; the concentration of $HCitrate^{2-}$ was calculated on the basis of the pH and the total amount of citrate in the sample. We used the following pK values for transition between the different forms of citrate: 3.15, 4.77, and 6.40.[25]

$$f_A = \frac{1}{1 + X(1,1) + X(1,2) + X(1,3) + K\cdot X(1,1)}$$

$$f_B = \frac{1}{Y(1,1) + 1 + X(2,2) + X(2,3) + K}$$

$$f_C = \frac{1}{Y(1,2) + Y(2,2) + 1 + X(3,3) + K\cdot Y(2,2)}$$

$$f_D = \frac{1}{Y(1,3) + Y(2,3) + Y(3,3) + 1 + K\cdot Y(2,3)}$$

$$f_E = \frac{K}{Y(1,1) + 1 + X(2,2) + X(2,3) + K}$$

$$X(v,w) = 10^{\sum_{i=v}^{w} -n_i\cdot(pK_i - pH)}$$

$$Y(v,w) = 10^{\sum_{i=v}^{w} n_i\cdot(pK_i - pH)}$$

$$K = \frac{[HCitrate^{2-}]}{K_{citr}} \qquad (1)$$

Data Analysis: Kinetic. To analyze the pH dependence of the recovery rate at different citrate concentrations, we assumed that this rate is directly related to the fraction of each species of pB. Therefore, we assigned a rate constant to each species of pB, as indicated by eq 2. Here the fraction of each species (f_A through f_E) is obtained from eq 1. Furthermore, the rate constant for the pB_m/pG′ mixture (k_B) is pH dependent.[14]

$$k = k_A\cdot f_A + k_B\cdot f_B + k_C\cdot f_C + k_D\cdot f_D + k_E\cdot f_E$$

$$k_B = \frac{k_{B,high} - k_{B,low}}{1 + 10^{n_B\cdot(pK_B - pH)}} + k_{B,low} \qquad (2)$$

Data Analysis: Parameter Confidence. Confidence intervals were determined, for the parameters used in the spectral and kinetic analysis, according to a method described elsewhere.[26] In short, confidence intervals were determined by varying the value of the parameter around the calculated optimum, and subsequently reoptimizing the other parameters. The values of the parameter were subsequently plotted against the sum square error (SSE) of the reoptimized analysis. Obtained plots generally have a parabola-like shape, with the optimum value at the minimum (see Figure S8, Supporting Information,

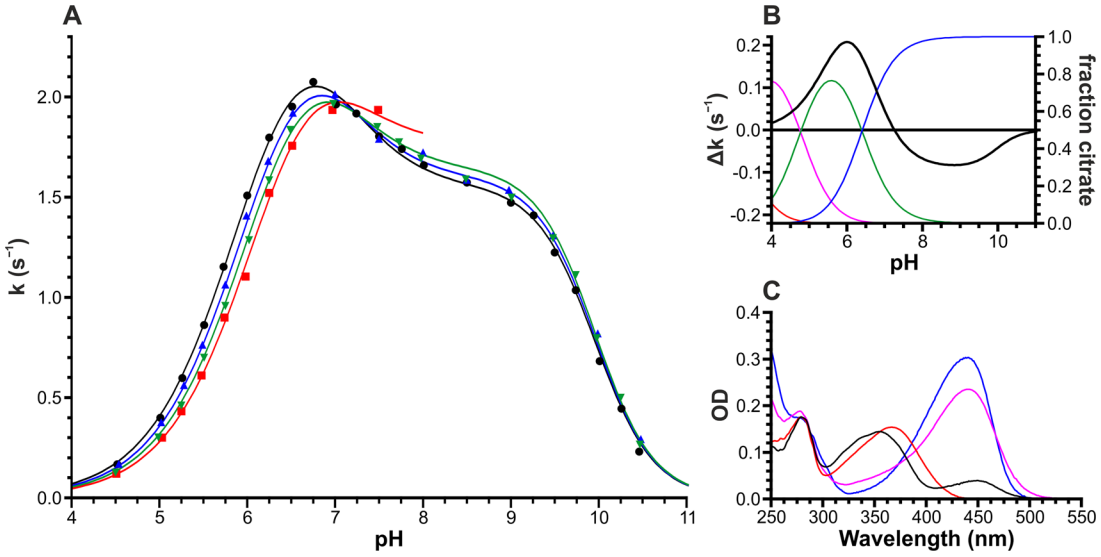

Figure 1. Initial analysis of WT PYP. Panel A: Kinetic analysis of pH dependent recovery rate in the presence of varying amounts of citrate. 0 mM citrate (disk; black), 10 mM (triangle up; blue), 20 mM (triangle down; green), 30 mM (square; red). Fitted lines are best fits through the data; i.e., no parameter constraints were used. Panel B: Left axis, difference curve (solid line; black) of two fit curves from panel A (0–20 mM citrate). Right axis, fraction of citrate species H_3Citrate (red), H_2Citrate$^-$ (magenta), HCitrate^{2-} (green), and Citrate^{3-} (blue). Panel C: Spectral analysis of pH dependent pB spectra at 0 mM citrate. From low to high pH, the spectral line colors are red, black, magenta, and blue.

for an example). The confidence interval was subsequently determined by setting a threshold SSE value (using a Fisher's F distribution).

Guanidine HCl Denaturation. Measurements were performed at 25 °C and pH 6.0 using the previously described buffer (see Sample/Buffer Preparation). Buffers with varying amounts of guanidine HCl were prepared by mixing buffers containing 0 and 5.5 M guanidine HCl. The guanidine HCl concentration was determined via the refractive index of the buffer solution.[27] The same spectrophotometer setup as described above was used to record spectra. For further details, see the Supporting Information.

NMR Measurements. Solution-NMR spectra were recorded on a Bruker AvanceII 500 MHz spectrometer operating at a ^{1}H frequency of 500 MHz. NMR samples of uniformly [^{15}N]-labeled WT PYP were prepared in Shigemi tubes, containing 200 μL of 0.6 mM protein in 20 mM buffer solution (90% H_2O/10% D_2O, 150 mM NaCl, pH 6.2), both in the absence and presence of 20 or 50 mM sodium citrate. DSS (0.2 mM) was used as an internal chemical shift reference. 1D proton spectra and sensitivity enhanced 2D ^{15}N–^{1}H HSQC spectra[28] were recorded at 38 and 53.5 °C. For further details, see the Supporting Information.

Autodock Calculations. Docking of HCitrate^{2-} on PYP was carried out using the Autodock 4.0[29] routine that has been implemented in Yasara Structure version 10.11.8. The high-resolution 0.82 Å crystal structure 1nwz.pdb[30] was used for pG. The same structure was used to generate a simplified model for the structure of pB, where the amino acids 1–18 were deleted. In addition, the ensemble structure 2kx6.pdb[31] was used for pB. For further details, see the Supporting Information.

RESULTS

We have extended our previous work on WT PYP,[14] by measuring the pH dependency of the photocycle recovery rate over a large pH range (4.5–10.5) in the presence of citrate. As before, we have kept the temperature, ionic strength, and buffer composition constant and varied only the pH and citrate concentration (0, 10, 20, and 30 mM). It should be noted that with 30 mM citrate we could only measure up to pH 7.5, as it was not possible to keep the ionic strength at 250 mM above this pH in the presence of 30 mM citrate. Furthermore, we have carried out the same set of measurements with the mutant derivatives H108F[32] and Δ25.[33]

WT PYP: Initial Analysis. We confirmed the observation for WT PYP that at low pH the presence of citrate retards the recovery reaction of PYP.[20] When we look at the pH dependence of the recovery kinetics, the pH transition of these kinetics appears to shift toward higher pH with increasing citrate concentration (see Figure 1A). We fitted the data points using the model from our previous work.[14] To visualize the citrate induced change, we subtracted the fitted curve from Figure 1A at 20 mM from the one at 0 mM citrate. Comparison with citrate titration curves (see Figure 1B) revealed that the citrate induced retardation seems to correlate specifically to the presence of hydrogen-citrate (i.e., HCitrate^{2-}). It is therefore likely that this species retards the photocycle recovery rate. The slight discrepancy between the maxima for HCitrate^{2-} and the retardation effect in Figure 1B is likely caused by a difference in influence of HCitrate^{2-} on the different pB subspecies.

At higher pH (>7.5), i.e., the pH range in which Citrate^{3-} is most abundant, the addition of citric acid has the opposite effect: consistently a small acceleration of the recovery reaction is observed. Because of its small size, this effect has not been further analyzed.

In our previous work, we linked the pH transition of the recovery rate to the pH transition of pB spectra.[14] In this previous study, we obtained a low pH pB spectrum (pB$_l$; λ_{max} ~368 nm), a medium pH pB spectrum (mixture of pB$_m$ with λ_{max} ~355 nm, and pG′ λ_{max} ~450 nm), and a high pH pB spectrum (pB$_h$; λ_{max} ~430 nm). One might therefore expect the transition of the low to medium pH pB spectra to shift to higher pH as well. However, in our initial analysis, the spectral pH transition appeared to shift to lower pH, i.e., in the opposite direction of the shift of the kinetic pH transition. It was therefore clear to us that our relatively simple photocycle scheme no longer sufficed to analyze pH dependent photocycle events in the presence of citrate.

dx.doi.org/10.1021/jp306891s | J. Phys. Chem. B 2012, 116, 13172–13182

In our previous work, we noted that in all likelihood there is an additional spectral transition for pB at high pH, caused by deprotonation of tyrosine residues. Improvements in our analysis protocol have allowed us to confirm the presence of this transition. As a result, we now include two high pH pB subspecies instead of just one (i.e., pB_h now becomes pB_{h1} and pB_{h2}). The resulting spectra for each subspecies of pB are shown in Figure 1C.

WT PYP: Incorporation of the Influence of Citrate into the Photocycle Model. For the incorporation of the influence of citrate into our photocycle model, we have used the following criteria and assumptions, which are based on our initial analysis. The influence of citrate on PYP is caused by $HCitrate^{2-}$. $HCitrate^{2-}$ only influences PYP when it can bind to a relatively unfolded form of PYP, i.e., the pB form that dominates at medium pH (pB_m). When $HCitrate^{2-}$ is bound to pB, the latter can no longer form pG′. Effectively, this leads to the addition of a $HCitrate^{2-}$ bound pB intermediate (pB_{citr}), which is in equilibrium with pB_m (see Figure 2). As such, our pH dependency model for pB has changed from a basic single species with two pH transitions model[14] to one that has three pH transitions plus a $HCitrate^{2-}$ dependent equilibrium. Here we should be able to distinguish spectra for pB_l, (pB_m + pG′), pB_{h1}, pB_{h2}, and pB_{citr}. Note that pB_{citr} and pB_m are expected to have similar spectral characteristics, with one difference: the pB_m intermediate cannot be distinguished from pG′. Furthermore, by introducing an additional pB species at high pH, we can no longer assume that only the pB_m + pG′ mixture contributes significantly to the recovery rate. As such, the recovery rate is determined by summing the fraction of each subspecies of pB multiplied by its representative recovery rate. Note that only the recovery rate linked to the pB_m + pG′ mixture is pH dependent (see eq 2). Also, this pH dependent rate should have a significantly higher value than the other rate constants. Simulations with this model (eqs 1 and 2) confirm that with increasing citrate concentration the pH dependence of the presence of pG′ shifts to higher pH, while the transition from (pB_m + pB_{citr}) to pB_l shifts to lower pH.

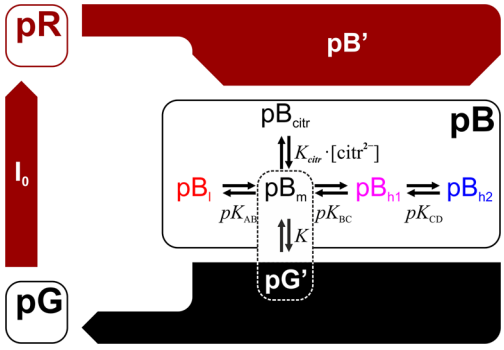

Figure 2. Photocycle scheme of PYP indicating pH and citrate dependence of pB species. In this scheme, the three basic photocycle species pG, pR, and pB are indicated by boxes. Inside the box of the pB species, a scheme is shown for the distribution of pB subspecies as a function of pH and citrate, where pB_l, pB_m, pB_{h1}, and pB_{h2} represent subspecies of pB that dominate at low, medium, and high pH, respectively. As pK_{BC} and pK_{CD} differ only modestly (~1 pH unit; see Table 1), we introduced two subspecies with subscript h for high pH (i.e., h1 and h2). pB_{citr} represents a subspecies of pB that has $HCitrate^{2-}$ bound to it, and is exclusively formed via an equilibrium with pB_m. The solid arrows between the boxes of the basic photocycle species indicate the route of the photocycle. Intermediates that may be involved in the transition from one basic species to the other are indicated inside these solid arrows. Note that depending on the conditions these intermediates may or may not be involved. For example, pG′ is only involved if the transition of pB to pG goes through the pB_m subspecies of pB. If the transition of pB to pG goes through any of the other subspecies of pB, pG′ is not involved. The part of the photocycle we focus on in the work presented here is indicated by the black boxes (pB and pG) and the black arrow between the pB and pG boxes; the other parts are shown in dark red.

Analysis of the data with the model incorporating citrate would benefit from a global approach that includes all data sets in a single analysis and combines kinetic and spectral analysis. However, at this time, this is not possible due to the size of the complete data set, as well as minor differences in scaling between data sets recorded under a multitude of conditions. As such, we were forced to apply the model on subsets of the data. To retain the required global aspect in the analysis, we made the following assumptions: (i) The pK's of the transitions between the different subspecies of pB are constant between subsets of data. (ii) The pK values for transition between the different forms of citrate are 3.15, 4.77. and 6.40[25] and have a cooperativity constant of 1. (iii) The binding constant for the binding of $HCitrate^{2-}$ to pB_m is constant between subsets of data. (iv) The pH dependence of the recovery rate, which is linked to the fraction pB_m/pG′, is not dependent on the citrate concentration. (v) The model parameters should allow for a good fit through both kinetic and spectral aspects of the data set.

WT PYP: Analysis with Citrate-Incorporated Model. As a starting point, we used the spectral analysis in the absence of citrate. The parameters obtained from this analysis cannot be influenced by citrate and therefore conform to our constraint that these parameters are not citrate dependent. Subsequently, a kinetic analysis was performed, which allowed us to fit data measured as a function of both pH and citrate concentration in a single global fit. In this analysis, all parameters related to the transition between the different subspecies of pB and citrate were fixed, with the exception of the binding constant of $HCitrate^{2-}$ to pB_m. The result of this analysis is summarized in Table 1. When these values for the model parameters were applied to the pH dependent spectral data in the presence of citrate, a reasonably good description of the data was obtained (data not shown). The resulting spectrum for pB_{citr} is indeed similar (not identical) to pB_m, only without the contribution of pG′ (data not shown).

H108F-PYP Analysis. Since citrate appears to bind only to PYP's pB_m subspecies, we decided to determine the effect of citrate on the H108F mutant of PYP. This mutant seems to undergo less structural change upon formation of pB.[32] Therefore, it may not be able to bind citrate, or behave differently in the presence of citrate.

The analysis of the data obtained for H108F PYP was done in the same way as for WT PYP. However, the analysis proved to be less straightforward than that of WT PYP. The confidence intervals for the pK_{CD}, n_{CD}, and K_{citr} parameters turned out to cover a very large range, indicating they could not be determined from the current data set. Therefore, for the pK_{CD} and n_{CD} parameters, values obtained for WT PYP were used. The K_{citr} parameter was fixed to a value (100 M) that basically removes the influence of citrate from the model. As a result, the parameter k_E could also be fixed (to 0 s^{-1}), as it should have no influence in the model anymore. However, to determine the lower limit of the K_{citr} parameter, the parameter k_E was not fixed. The results from this analysis are collected in Figure 3 and Table 1. Notably, the

dx.doi.org/10.1021/jp306891s | J. Phys. Chem. B 2012, 116, 13172−13182

Table 1. Analysis Results with pH and Citrate Dependent Model for the Rate of PYP Recovery[a]

transition[b]				kinetic[c]			
	fit	lower limit	upper limit		fit	lower limit	upper limit
				WT PYP			
pK_{AB}	5.955	5.950	5.960	k_A	0.08	0.04	0.13
pK_{BC}	9.87	9.85	9.88	pK_B	7.0	6.8	7.1
pK_{CD}	10.56	10.51	10.62	n_B	1.0	0.8	1.3
n_{AB}	1.04	1.03	1.05	$k_{B,low}$	2.8	2.6	3.1
n_{BC}	1.18	1.17	1.19	$k_{B,high}$	1.62	1.56	1.67
n_{CD}	1.6	1.5	1.7	k_C	0.24	0.16	0.32
K_{citr}	0.06	0.05	0.09	k_D	0.0	*0*	0.10
				k_E	0.0	*0*	0.30
				H108F PYP			
pK_{AB}	5.41	5.38	5.43	k_A	0.00	*0*	0.0084
pK_{BC}	9.51	9.50	9.52	pK_B	6.9	6.7	7.0
pK_{CD}	*10.564*			n_B	0.9	0.7	1.3
n_{AB}	0.74	0.72	0.77	$k_{B,low}$	0.69	0.67	0.72
n_{BC}	0.865	0.859	0.872	$k_{B,high}$	0.47	0.45	0.48
n_{CD}	*1.6*			k_C	0.05	0.02	0.07
K_{citr}	*100*	0.16		k_D	0.00	*0*	0.065
				k_E	*0*		
				Δ25-PYP			
pK_{AB}	*1*			k_A	*0*		
pK_{BC}	9.27	9.26	9.29	pK_B	7.1	6.7	7.7
pK_{CD}	10.17	10.13	10.25	n_B	1.0	0.4	
n_{AB}	*1*			$k_{B,low}$	0.0042	0.0039	0.0045
n_{BC}	0.92	0.91	0.93	$k_{B,high}$	0.0061	0.0057	0.0071
n_{CD}	1.5	1.3	1.7	k_C	0.020	0.019	0.021
K_{citr}	*100*			k_D	0.0176	0.0169	0.0182
				k_E	*0*		

[a]Values that were forced are depicted in italic. The unit of K_{citr} is M. The unit of the rate constants (k_x) is s^{-1}. [b]Parameters in the transition column were determined via pH dependent spectral analysis in the absence of citrate, with the exception of the K_{citr} parameter, which was based on global analysis of kinetic data. [c]Parameters in the kinetic column were determined via a global analysis of kinetic data.

lower limit for K_{citr} (160 mM) is still significantly higher than the WT value for K_{citr} (63 mM).

Other major differences with the WT data are that the pK transition between subspecies of pB at low pH has shifted to a lower pK by ~0.5 pH units. A similar shift was observed for this mutant when monitoring the pH dependent proton uptake and release upon illumination.[34] Furthermore, the contribution of pG′ in the mixed pB_m/pG′ spectrum is significantly less compared to that in WT PYP, as we noted previously.[14] Lastly, from the obtained rate constants for H108F PYP (see Table 1), it is clear that recovery of H108F is significantly slower than WT PYP.

Δ25-PYP Analysis. Since there is a good chance that the N-terminus is involved in citrate binding, we decided to also determine the effect of citrate on the Δ25 mutant of PYP. In this mutant, the N-terminus is absent. Due to the very slow recovery kinetics of this mutant, we added a neutral density filter between the light source of the spectrophotometer and the sample, to minimize probe light induced photocycle activation. As a result, we were no longer able to reliably record spectral information below 300 nm.

The analysis of the data obtained for Δ25-PYP ground state recovery shows no sign of being influenced by citrate. For the analysis of Δ25-PYP recovery, we were only able to detect pH induced transitions at high pH; the low pH transition around pH 6 appears to be absent in Δ25-PYP (see Figure 4). As a result, we had to adjust the analysis models. The spectral analysis at 0 mM citrate was performed with a simple 2 pH transition model. For the subsequent kinetic analysis, the low pH transition was fixed at a pK of 1, effectively removing the influence of the pB_l species from the model in the pH domain we analyzed. Also, K_{citr} was set to 100 M to remove the influence of citrate from the model. Additionally, the rates k_A and k_E were fixed to 0 s^{-1}, as they should have no influence in the model. Again, the parameters obtained from the spectral analysis at 0 mM citrate were used (fixed) in the global analysis of the pH-dependent kinetic data (see Figure 4 and Table 1). Note that the low pH spectrum for pB of Δ25-PYP is similar to the pB_m spectra of WT and H108F PYP. Also, recovery is slower for this pB_m species than pB_{h1}. The contribution of pG′ in the pB_m spectra is very low. Furthermore, the pH dependence of k_B remains, although, in contradiction with the WT and H108F data, the rate is slower at low pH. Removing the pH dependence of k_B results in a poor fit (data not shown), indicating this pH dependence is not destroyed when removing the N-terminus from PYP.

Protein Stability. The citrate induced slower recovery of WT PYP can be interpreted as a stabilization of the pB structure by citrate. Therefore, we determined the relative stability of WT, H108F, and Δ25-PYP (both in their pG and pB forms) in the absence and presence of citrate via guanidine HCl titrations. The results are summarized in Table 2. Interestingly, based on ΔG_0 alone, citrate only has a clear stabilizing impact on the protein's conformational stability in pG of Δ25-PYP and destabilizes WT in pG. For pB, no significant stabilization by citrate is observed. Therefore, the retardation of pG recovery in the presence of citrate is likely not caused by a stabilizing effect of citrate.

dx.doi.org/10.1021/jp306891s | J. Phys. Chem. B 2012, 116, 13172−13182

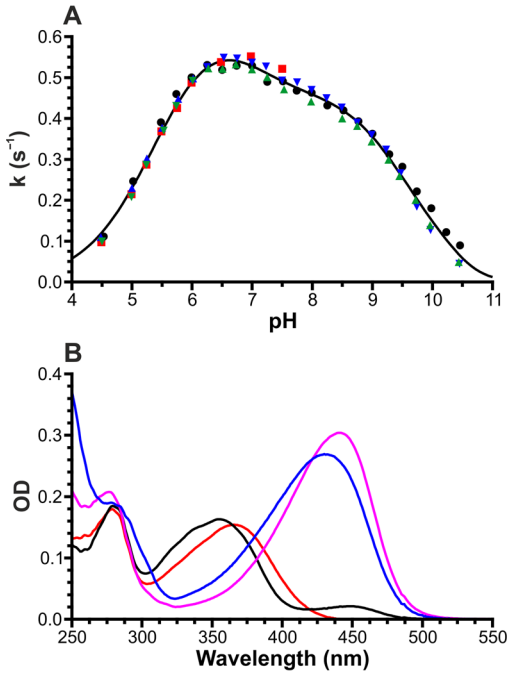

Figure 3. Analysis of H108F PYP. Panel A: Kinetic analysis of pH dependent recovery rate in the presence of varying amounts of citrate. 0 mM Citrate (disk; black), 10 mM (triangle up; blue), 20 mM (triangle down; green), 30 mM (square; red). The fitted line is the global fit at 0 mM citrate using our photocycle model that includes the influence of citrate (see Table 1 for model parameters). Fitted lines at 10, 20, and 30 mM are highly similar and are therefore not shown. Panel B: Spectral analysis of pH dependent pB spectra at 0 mM citrate. From low to high pH, the spectral line colors are red, black, magenta, and blue.

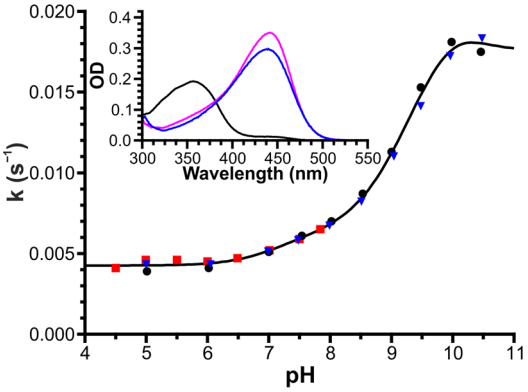

Figure 4. Analysis of Δ25-PYP. Kinetic analysis of pH dependent recovery rate in the presence of varying amounts of citrate. 0 mM Citrate (disk; black), 20 mM (triangle down; green), 30 mM (square; red). The fitted line is a global fit at 0 mM citrate using our photocycle model that includes the influence of citrate (see Table 1 for model parameters). Inset: Spectral analysis of pH dependent pB spectra at 0 mM citrate. From low to high pH, the spectral line colors are red, black, magenta, and blue.

When we look at the $[Gnd]_{1/2}$ parameter, a consistently higher value is observed in the presence of citrate, with the single exception of the pG form of WT PYP. This indicates that the denaturant and citrate compete, at least in part, for the same binding sites. Furthermore, in pB of WT and H108F, the shift is larger (~0.3−0.4 mM) compared to the shift under the other conditions (~0.1 mM). This is consistent with the disruption of the N-terminus in pB.

Finally, the *m* value is interesting in the sense that it represents the change in solvent accessible surface area (SASA) upon denaturation.[35] Here a higher *m* value represents a larger change in SASA. As might be expected, between pG and pB, the *m* value is consistently smaller in pB, even in Δ25-PYP. Furthermore, citrate seems to consistently decrease the *m* value in WT and H108F, while no significant change is observed for Δ25-PYP. This indicates that citrate may have a disruptive effect on the N-terminus of PYP.

Solution-NMR Analysis of Citrate Binding. To get more detailed information about a possible binding site for citrate, we performed several solution-NMR measurements on WT PYP. Experiments were performed in the presence and absence of citrate at pH 6.2. Assignment of individual amides in the ground state (pG) follows from 3D NOESY spectra, while corresponding assignments in the pB state were made at a higher temperature than in previous studies[36] to eliminate the conformational line broadening that hampered resonance assignments of the pB state of WT PYP. Details of the assignments for pB at high temperature will be described elsewhere.

Titration up to 20 mM citrate does not reveal any chemical shift perturbation of amide protons in the spectra of the pG state at 38 °C. Only at 50 mM citrate and a higher temperature (53.5 °C), small perturbations are seen just above the detection limit of 0.003 ppm (see Figure 5A). The largest changes (up to 0.04 ppm) are observed for amino proton HE22 of Q32 and amides F6, F28, and R124. The amides in loop regions around L88-N89 and G112-S117 are perturbed up to 0.02 ppm. In conclusion, citrate displays very weak binding toward the pG state of PYP.

In contrast, a clear citrate-induced difference can be observed in the HSQC spectrum of the pB intermediate, recorded under similar conditions as for pG (see Figure 5B). Chemical shift changes of pB in the presence of citrate amount up to 0.06 ppm and are spread over the entire protein sequence. The most pronounced perturbations, however, are observed for amides in the important helical region (44−51), and the beta strand regions (90−99 and 103−110). Also, the N-terminal region at positions G25 and G29 is disturbed relatively strongly in the pB state after binding of citrate. Figure 5B shows that the first 19 amino acids of the N-terminus remain largely invisible despite the much improved spectral quality of the HSQC spectra of pB at elevated temperature. Possibly, the loss of secondary structure in the N-terminus of pB causes an increased solvent-exchange rate of these amides that results in diminished proton signals. From the titration data on pB, it is concluded that $HCitrate^{2-}$ may bind to either the junction between the N-terminal side and helix (44−51) of PYP and/or the exterior side of the two long β-sheets (88−97 and 103−111) that are bridged by a hairpin loop. Either way, the NMR perturbation data indicate that almost the whole structure of the pB molecule is affected by binding of citrate.

Docking Studies of Citrate Binding. In order to independently search for possible binding positions of $HCitrate^{2-}$ (see Figure 6E) on the surface of the pG and pB states of PYP, we performed a docking study at pH 6.2 using Autodock. The docking results on pG are schematically displayed in Figure 6A. The four main clusters indicated by roman numerals point to binding sites that are complementary to the negatively charged citrate molecule. In summary, the preferred binding positions are located at (**I**) in the loop pocket surrounded by K17, W119, L113, S114, and the side chain of Q32, (**II**) near F6 and the side chains of K106 and K123, (**III**) near side chains of K123 and R124, and (**IV**) in the loop region

dx.doi.org/10.1021/jp306891s | *J. Phys. Chem. B* 2012, 116, 13172−13182

Table 2. PYP Conformational Stability Based on Guanidine Denaturation

	pG		pB	
[citrate]	0 mM	52 mM	0 mM	52 mM
		WT PYP[a]		
$[Gnd]_{1/2}$ (M)	2.616 (2.614–2.617)	2.547 (2.546–2.548)	1.92 (1.91–1.93)	2.36 (2.32–2.40)
m value ($kJ \cdot mol^{-1} \cdot M^{-1}$)	17.4 (17.2–17.5)	16.6 (16.5–16.7)	13.9 (13.4–14.4)	12.0 (10.6–13.6)
ΔG_0 ($kJ \cdot mol^{-1}$)	45.4 (45.0–45.9)	42.3 (42.0–42.6)	26.6 (25.6–27.7)	28.2 (24.6–32.7)
		H108F PYP[a]		
$[Gnd]_{1/2}$ (M)	2.532 (2.530–2.533)	2.626 (2.625–2.628)	2.25 (2.24–2.27)	2.58 (2.56–2.60)
m value ($kJ \cdot mol^{-1} \cdot M^{-1}$)	16.0 (15.8–16.1)	15.5 (15.3–15.6)	7.7 (7.3–8.1)	7.0 (6.7–7.4)
ΔG_0 ($kJ \cdot mol^{-1}$)	40.4 (40.0–40.7)	40.6 (40.2–40.9)	17.3 (16.3–18.3)	18.2 (17.3–19.2)
		Δ25-PYP[a]		
$[Gnd]_{1/2}$ (M)	2.062 (2.060–2.064)	2.120 (2.119–2.122)	2.02 (1.99–2.04)	2.16 (2.14–2.18)
m value ($kJ \cdot mol^{-1} \cdot M^{-1}$)	14.3 (14.2–14.5)	14.4 (14.2–14.5)	7.5 (7.1–8.0)	7.5 (7.0–7.9)
ΔG_0 ($kJ \cdot mol^{-1}$)	29.5 (29.2–29.9)	30.4 (30.2–30.7)	15.2 (14.1–16.4)	16.1 (14.9–17.2)

[a]Conformational stability was determined for WT, H108F, and Δ25-PYP at pH 6.0 for both the pG and pB forms at 0 and 52 mM citrate. Values in parentheses indicate the 95% confidence interval for the fit parameters.

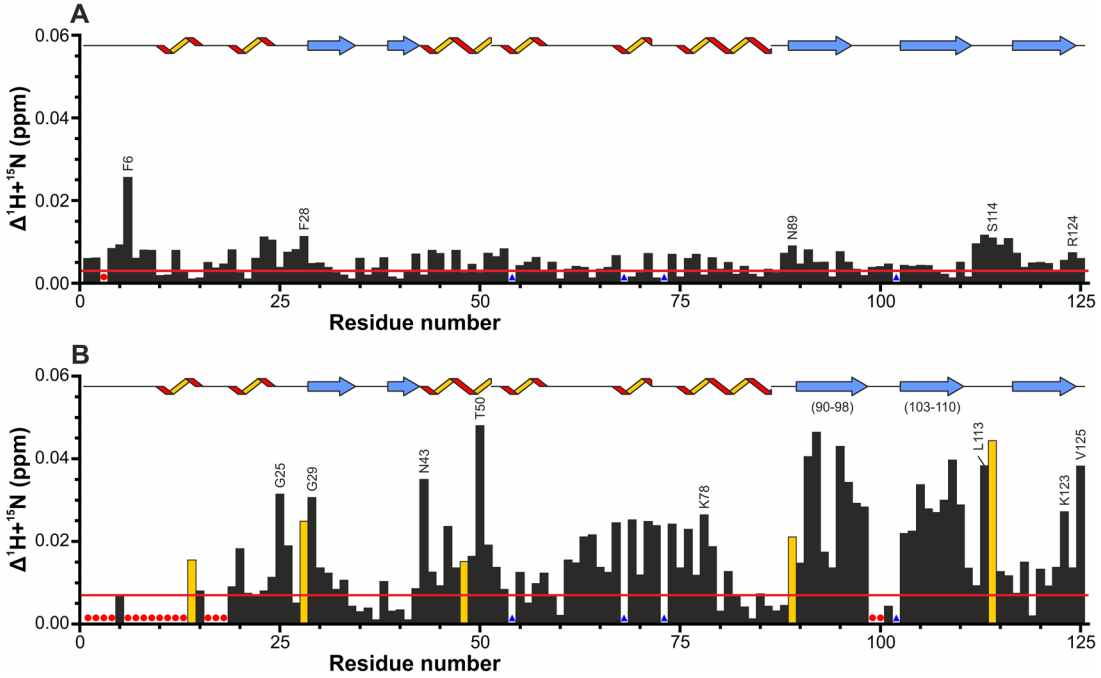

Figure 5. Chemical shift perturbations of amide proton pairs in the pG state (panel A) and the pB state (panel B) in the presence of 50 mM citrate. Absolute chemical differences $\Delta^1H + {}^{15}N$ are calculated as root-mean-square differences weighted according to $\sqrt{(\delta^1H)^2 + (\delta^{15}N/6.515)^2}$. Missing data points due to high-solvent exchange rates or exchange broadening are indicated by small red circles, and blue triangles correspond to proline positions. Yellow bars in panel B show amides for which less accurate delta values are calculated, mostly due to partial overlap of amide protons in the compared NMR spectra, or by low sensitivity of peaks in the noncitrate reference spectrum. The red horizontal lines give the estimated average limit for which significant chemical shift differences can still be measured accurately (>0.003 and >0.007 ppm for pG and pB, respectively). The secondary structure cartoon displayed at the top of the diagrams is derived from the crystal structure of pG (1nwz.pdb).[30] See Figure S9 (Supporting Information) for the $^{15}N-^1H$ spectra.

adjacent to N87 and L88. In fact, the amide protons that are predicted to ligate to citrate correspond to the slight perturbations observed in the HSQC spectra. Thus, despite the low-affinity binding of citrate, these calculations are in full agreement with the experimental observations. Docking results on the pB structure are difficult to obtain, as at the time of this writing no solution structure of the pB state of WT PYP at atomic resolution was available. What we do know is that the structure of the pB state is less ordered than that of pG, especially in the N-terminus. To get an impression of the situation in WT PYP pB, we opted to test two structures, one a simplified model based on the pG structure and the other an ensemble structure for pB based on various structural probes.[31]

For the simplified model of pB, we use a truncated model (Δ1–18) derived from the pG crystal structure, in which the coordinates of 18 amino acids of the N-terminus are removed. This is based on the lack of amide proton signals from these 18 amino acids in the HSQC spectra at high temperature. The docking results for the simplified model of pB are shown in Figure 6B and C. The removal of the N-terminal residues leads to a newly available positively charged surface patch (**I**) that is normally occluded in the pG state by the aromatic ring of F6. The amino acids involved in this pocket are located on the β sheet

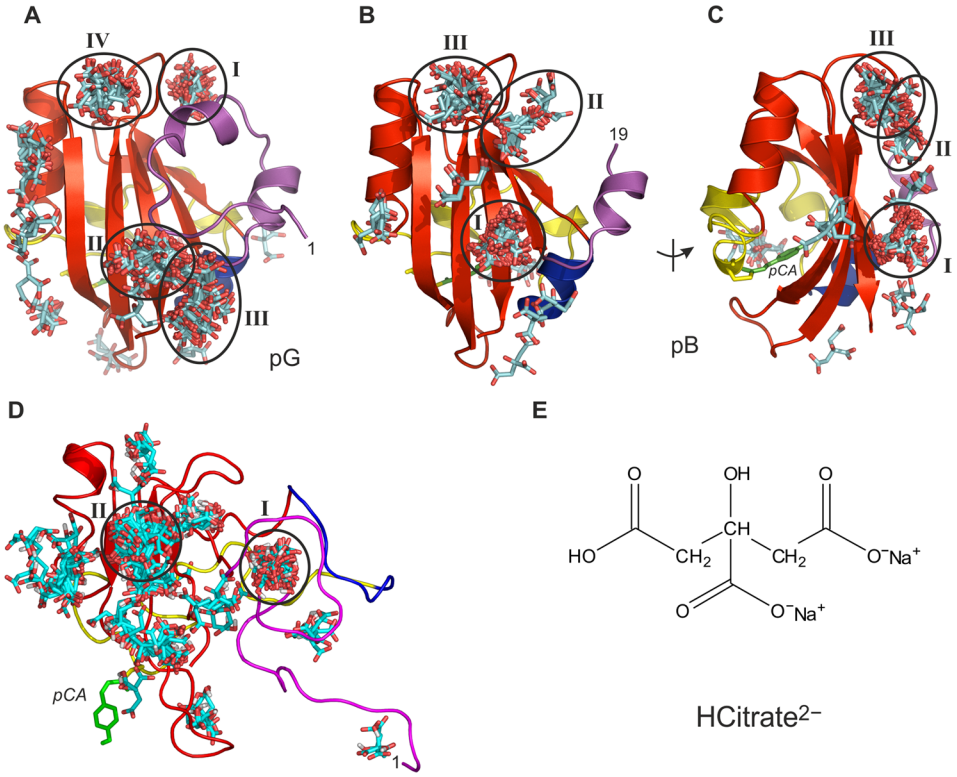

Figure 6. Autodock results of docked divalent citrate (see also the structural formula in panel E) on the pG and pB structures. Citrate docking orientations of the best 200 solutions are shown as clusters. Circles indicate the position of the most favorable docking solutions, sequentially ordered with roman numerals going from high to low binding energy. The chromophore pCA covalently attached to Cys69 is indicated in green. The N-terminus (residues 1−28) is colored magenta, and the backbone in red (29−43, 75−125), blue (44−51), and yellow (52−74) shows the corresponding structure of both pG and pB. Panel A: Front view of pG (1nwz.pdb, 0.82 Å crystal structure[30]). Panels B and C: Front and side views, respectively, for a simplified pB model that is compatible with the NMR structure in solution (a truncated Δ(1−18) pG). Panel D: Ensemble pB structure (2kx6.pdb, based on various structural probes[31]). Panel E: Structural formula of sodium citrate in its $HCitrate^{2-}$ state. Note that the molecule has symmetric carboxylate end groups. For a schematic representation of the possible binding sites indicated by roman numerals in panels A−D, see Figure S10 (Supporting Information).

surface and include protonated H108, K106, K110, and K123. Cluster **I** is the dominant docking solution (74%) found for the simplified pB model; other docking solutions of citrate are less favorable in energy and converge to similar surface positions already seen for the nontruncated structure of pG. Interestingly, the cluster **I** binding position can be made accessible in pG by simply rotating the ring and backbone of F6 out of the way (see the Supporting Information).

A structure for pB that recently became available (2kx6.pdb) is an ensemble structure that is based on data from a multitude of techniques and PYP mutants, that were recorded under varying conditions.[31] Also for this structure, multiple binding possibilities were found (Figure 6D). Clusters **I** (27%) and **II** (30%) are the dominant docking solutions. Docking cluster **I** is located in an open type loop in the N-terminal domain consisting mostly of hydrogen bonds to the amide backbone involving residues K17, L23, and L26-F28. Docking cluster **II** involves H108, a residue also found in the simplified model of pB, and is located on the N-terminal side of the central β-sheet.

DISCUSSION

An extensive amount of knowledge already exists about the bio/photophysics of PYP. As a result, various versions of its photocycle have appeared over the years to try and describe how PYP functions. We have found that it helps to interpret the photocycle based on just three key species (pG, pR, and pB). The key is that each of these species should be considered a large ensemble of similar but ultimately different structures. This is of course not a radically new idea; it is just the consequence of the dynamic nature of proteins.[37,38] Each ensemble of species can subsequently be subdivided in subensembles that may dominate under specific conditions, e.g., in a specific pH range.

For this study, we have generated an extensive data set to study the recovery characteristics of PYP as a function of both pH and citrate concentration. It has already been established that citrate retards ground state recovery of PYP at low pH.[20] By varying both pH and the concentration of citrate, we aimed to determine if the influence of citrate is general or linked to a specific species of citrate. On the basis of our experiments, we have learned that specifically hydrogen-citrate ($HCitrate^{2-}$) slows down PYP recovery between pH 4.5 and 7. Furthermore, it only influences a specific subset of pB (pB_m), which dominates between pH 6 and 10.

Additionally, at pH > 7.5, there appears to be a slight citrate induced acceleration of PYP recovery. This effect is rather small, however, and is likely linked to the $Citrate^{3-}$ species. In order not to overly complicate the photocycle model, we ignored the influence of $Citrate^{3-}$. Significantly though, solution-NMR measurements at pH 7.9 revealed that $Citrate^{3-}$ may bind to the same surface region of the β-sheet of PYP that is exposed in the signaling state (data not shown).

By treating the pB intermediate as an ensemble of subspecies, it was fairly straightforward to incorporate the influence of

dx.doi.org/10.1021/jp306891s | J. Phys. Chem. B 2012, 116, 13172−13182

$HCitrate^{2-}$ on the photocycle. All that basically was required was to add an equilibrium reaction for the binding of $HCitrate^{2-}$ to the pB_m subspecies. This equilibrium is suggested by the data through the observed influence of citrate, which appears to be linked to both the presence of $HCitrate^{2-}$ and pB_m (see Figure 1B). As a result, we were able to determine an equilibrium constant for the binding of $HCitrate^{2-}$ to pB_m. It is clear that this equilibrium constant is greater in the H108F mutant of PYP. In other words, $HCitrate^{2-}$ appears to bind less efficiently to H108F PYP compared to WT PYP. Note that when the equilibrium constant of WT PYP was used in the analysis of H108F PYP anyway, not only did the fit of kinetic data become significantly worse, but also the spectral analysis resulted in clearly incorrect spectra (data not shown). Unfortunately, we were not able to perform these measurements at citrate concentrations above 30 mM. Due to the nature of citrate, a higher citrate concentration would also require a higher ionic strength of the sample. A test using an ionic strength of 1 M, instead of 250 mM, revealed that the influence of the higher ionic strength overshadows the influence of citrate and no citrate effect was visible anymore (see Figure S7, Supporting Information). As such, we were not able to determine the citrate binding constant very accurately (see Table 1 and Figure S8, Supporting Information). Interestingly, the H108 residue also showed up as a possible citrate interaction partner in our Autodock calculations, which could explain the lower binding affinity in H108F PYP.

Another aspect of the photocycle model we use here is the double transition at high pH for pB, signifying first deprotonation of the chromophore, resulting in a red-shift in the spectrum, followed by a transition signified by deprotonation of tyrosine residues. Data at high pH is difficult to measure and analyze, not only because of the relatively extreme solvent conditions required to measure these transitions but also due to the overlap of the pG and pB_h spectra. The values obtained for these high pH regions should therefore be considered approximate. Even so, it is still possible to see the typical absorption increase caused by tyrosine deprotonation, as also previously observed for pG.[14] Furthermore, recent NMR measurements[39] have shown that Y76 and Y98 have a pK of 10.2 in pG. It is likely these tyrosine residues are also involved in the transition we see here for pB at pK ~10.6.

The pH dependence of the recovery rate in the Δ25 mutant has the same high pH transitions that we see in WT PYP (and H108F PYP). However, an equivalent to the transition around pH 6 that is observed in WT PYP could not be detected for the Δ25 mutant within the pH range we analyzed. Notably, the spectrum of the low-to-medium pH range is similar to pB_m in WT PYP. This is further proof that the transition from pB_l to pB_m is caused by solvent exposure of the central β-sheet due to changes in the N-terminus. Since in the Δ25 mutant the central β-sheet is always solvent exposed, it is reasonable to expect that the pB spectrum at low to medium pH is similar to pB_m in WT PYP.

The experiments reported here were also initiated to obtain a better insight into the elusive pG′ intermediate. We already postulated that two elements are important for the properties of this intermediate, the protonation state of the chromophore (deprotonated) and the folding state of the protein.[14] The protonation state reveals itself spectrally. The importance of the folding state has now revealed itself through comparison of the WT, H108F, and Δ25-PYP results presented here. Previously, we postulated that the recovery rate is linked to the amount of pG′ that is present. In other words, the recovery rate is dependent on the equilibrium between pB_m and pG′. This fits nicely with what is observed in H108F PYP, where the recovery rate is slower than in WT PYP and where we observe less pG′ as well. However, if this is the only factor, we should not be able to observe pG′ for Δ25-PYP, which has a very slow recovery rate. The fact that we do observe a small amount of pG′ in this mutant indicates that recovery via pG′ is also significantly slower in this mutant. As the N-terminus is removed in Δ25-PYP, it is reasonable to assume the N-terminus plays an important role in recovery via pG′. Furthermore, as it is likely that the influence of pG′ is largely absent in Δ25-PYP, the recovery rate of this mutant may be representative for the direct recovery of pG from pB. It may therefore be interesting to have another look at mutants that severely influence the recovery rate characteristics such as the M100 mutants[40,41] and the E46Q mutant,[19,42] and investigate the possible role of pG′ in their behavior.

Binding of $HCitrate^{2-}$ to PYP is fairly specific. On the basis of the NMR experiments, it is clear that it binds—if at all—with very low affinity to the pG state but clearly perturbs spectra of the pB state (see Figure 5). On the basis of this chemical shift perturbation, it is likely that citrate anions bind between the central β-sheet and the N-terminus, which is only possible when the N-terminus moves away from the central β-sheet while forming the pB intermediate. This fits nicely with the observation that binding of $HCitrate^{2-}$ is specifically associated with the pB_m subset of pB, for which large structural changes, likely involving the N-terminus, have been proposed.[3,12,36]

Note that this does not mean citrate has no influence on pG. In fact, based on denaturation experiments, citrate seems to destabilize pG in WT PYP. Interestingly, where one can easily interpret the citrate induced slower recovery of WT PYP in pB as a stabilization of the pB structure by citrate, citrate appears to have no significant influence on the stability of pB. Therefore, the influence of citrate on the denaturation titrations seems mainly to be the result of competition for similar binding sites, and/or influencing the solvent accessible surface area of the protein. As such, the slower recovery rate that is observed in the presence of citrate in WT PYP is not so much a result of stabilization of a single pB state but more the result of a change in the distribution of the different subspecies of pB. In fact, we would suggest that changes in recovery rate can often be related to a change in distribution of pB subspecies. In addition, a change in the distribution of the different subspecies of pB may also explain the NMR perturbation data where small shift changes were observed in almost the whole pB structure.

A previously proposed binding site for anionic citrate near the chromophore pocket[20] of the pG state of PYP does not agree with our observation of a citrate binding site between the central β-sheet and the N-terminus. Therefore, we used the program Autodock[29] to obtain a more detailed impression of the site(s) where $HCitrate^{2-}$ may bind. The major problem here is the dynamic nature of pB, which makes it essentially impossible to assign a single structure to this intermediate. Therefore, we used two widely different structures for pB, each with their own pros and cons (see the Supporting Information). The analysis revealed several possible binding sites, none of which include the previously proposed binding site.[20] The most favored binding sites are indeed between the central β-sheet and the N-terminus, as we predicted on the basis of our measurements. Furthermore, for both pB structures, a binding site was found where H108 was involved. The involvement of H108 is in line with the observation that the influence of citrate in H108F PYP is either diminished or eliminated.

CONCLUSION

We have used the pH dependence of PYP as a tool to further refine the interpretation of the photocycle of this protein. To do this successfully, we deem it essential to interpret the "classic" photocycle intermediates/species of this protein as ensembles of subspecies. Here the distribution of these subspecies is dependent on characteristics such as pH. As a result, we were able to show that addition of citrate can influence photocycle recovery by influencing the distribution of pB subspecies. More specifically, we were able to show that $HCitrate^{2-}$ can interact with the pB_m subspecies to retard photocycle recovery. Furthermore, by doing the same for several mutants of PYP (H108F and Δ25), we could deduce that the relevant interaction of $HCitrate^{2-}$ with the pB_m subspecies was most likely situated between the central β-sheet and the N-terminus. This was then confirmed via NMR measurements and Autodock calculations.

The principles behind how citrate influences the PYP phototcycle may translate very well to how light signals received by PYP may be transduced to the cell, or how a transduction interaction partner for PYP may influence the photocycle of PYP *in vivo*, an aspect that has been very poorly characterized for PYP up to this point, especially since a transduction interaction partner for PYP may well interact at a similar place to where $HCitrate^{2-}$ interacts with pB_m, i.e., between the central β-sheet and the N-terminal cap.

We feel that the idea that changes in the distribution of photocycle intermediate subspecies influence photocycle kinetics and even the route taken in the photocycle reaction scheme is a powerful one that can and should be used in the (re)interpretation of PYP data.

ASSOCIATED CONTENT

Supporting Information

Extended Materials and Methods, a data analysis walkthrough, additional figures, and notes on, e.g., choices that were made in this study. This material is available free of charge via the Internet at http://pubs.acs.org.

AUTHOR INFORMATION

Corresponding Author

*Phone: +31-20-5257055. Fax: +31-20-5257934. E-mail: K.J.Hellingwerf@uva.nl.

Notes

The authors declare no competing financial interest.

ACKNOWLEDGMENTS

The authors thank J. C. Arents and J. van der Zwan for their expert technical assistance. This research has been supported by a grant from the HFSR program through grant number RPG0038/2006, The Netherlands Organisation for Scientific Research (NWO), and the EC FP6 Research Infrastructure Action program (project EU-NMR, contract # RII3-026145).

REFERENCES

(1) Hellingwerf, K. J.; Hendriks, J.; Gensch, T. *J. Phys. Chem. A* **2003**, *107*, 1082−1094.
(2) Cusanovich, M. A.; Meyer, T. E. *Biochemistry* **2003**, *42*, 4759−4770.
(3) van Brederode, M. E.; Hoff, W. D.; Van Stokkum, I. H.; Groot, M. L.; Hellingwerf, K. J. *Biophys. J.* **1996**, *71*, 365−380.
(4) Pellequer, J. L.; Wager-Smith, K. A.; Kay, S. A.; Getzoff, E. D. *Proc. Natl. Acad. Sci. U.S.A.* **1998**, *95*, 5884−5890.
(5) Taylor, B. L.; Zhulin, I. B. *Microbiol. Mol. Biol. Rev.* **1999**, *63*, 479−506.
(6) Van Beeumen, J. J.; Devreese, B. V.; Van Bun, S. M.; Hoff, W. D.; Hellingwerf, K. J.; Meyer, T. E.; McRee, D. E.; Cusanovich, M. A. *Protein Sci.* **1993**, *2*, 1114−1125.
(7) Baca, M.; Borgstahl, G. E.; Boissinot, M.; Burke, P. M.; Williams, D. R.; Slater, K. A.; Getzoff, E. D. *Biochemistry* **1994**, *33*, 14369−14377.
(8) Hoff, W. D.; Dux, P.; Hard, K.; Devreese, B.; Nugteren-Roodzant, I. M.; Crielaard, W.; Boelens, R.; Kaptein, R.; van Beeumen, J.; Hellingwerf, K. J. *Biochemistry* **1994**, *33*, 13959−13962.
(9) Kim, M.; Mathies, R. A.; Hoff, W. D.; Hellingwerf, K. J. *Biochemistry* **1995**, *34*, 12669−12672.
(10) Meyer, T. E.; Yakali, E.; Cusanovich, M. A.; Tollin, G. *Biochemistry* **1987**, *26*, 418−423.
(11) Xie, A.; Hoff, W. D.; Kroon, A. R.; Hellingwerf, K. J. *Biochemistry* **1996**, *35*, 14671−14678.
(12) Xie, A.; Kelemen, L.; Hendriks, J.; White, B. J.; Hellingwerf, K. J.; Hoff, W. D. *Biochemistry* **2001**, *40*, 1510−1517.
(13) Khan, J. S.; Imamoto, Y.; Yamazaki, Y.; Kataoka, M.; Tokunaga, F.; Terazima, M. *Anal. Chem.* **2005**, *77*, 6625−6629.
(14) Hendriks, J.; Hellingwerf, K. J. *J. Biol. Chem.* **2009**, *284*, 5277−5288.
(15) Shimizu, N.; Imamoto, Y.; Harigai, M.; Kamikubo, H.; Yamazaki, Y.; Kataoka, M. *J. Biol. Chem.* **2006**, *281*, 4318−4325.
(16) Otto, H.; Hoersch, D.; Meyer, T. E.; Cusanovich, M. A.; Heyn, M. P. *Biochemistry* **2005**, *44*, 16804−16816.
(17) Hoersch, D.; Otto, H.; Joshi, C. P.; Borucki, B.; Cusanovich, M. A.; Heyn, M. P. *Biophys. J.* **2007**, *93*, 1687−1699.
(18) Hendriks, J.; van Stokkum, I. H. M.; Hellingwerf, K. J. *Biophys. J.* **2003**, *84*, 1180−1191.
(19) Genick, U. K.; Devanathan, S.; Meyer, T. E.; Canestrelli, I. L.; Williams, E.; Cusanovich, M. A.; Tollin, G.; Getzoff, E. D. *Biochemistry* **1997**, *36*, 8−14.
(20) Shimizu, N.; Kamikubo, H.; Mihara, K.; Imamoto, Y.; Kataoka, M. *J. Biochem.* **2002**, *132*, 257−263.
(21) Kort, R.; Hoff, W. D.; Van West, M.; Kroon, A. R.; Hoffer, S. M.; Vlieg, K. H.; Crielaand, W.; Van Beeumen, J. J.; Hellingwerf, K. J. *EMBO J.* **1996**, *15*, 3209−3218.
(22) Hendriks, J.; Gensch, T.; Hviid, L.; van Der Horst, M. A.; Hellingwerf, K. J.; van Thor, J. J. *Biophys. J.* **2002**, *82*, 1632−1643.
(23) Düx, P.; Rubinstenn, G.; Vuister, G. W.; Boelens, R.; Mulder, F. A.; Hard, K.; Hoff, W. D.; Kroon, A. R.; Crielaard, W.; Hellingwerf, K. J.; Kaptein, R. *Biochemistry* **1998**, *37*, 12689−12699.
(24) Kraayenhof, R.; Schuurmans, J. J.; Valkier, L. J.; Veen, J. P. C.; Van Marum, D.; Jasper, C. G. G. *Anal. Biochem.* **1982**, *127*, 93−99.
(25) *Handbook of Chemistry and Physics*, 1st student ed.; Weast, R. C., Ed.; CRC Press, Inc.: Boca Raton, FL, 1988.
(26) Kemmer, G.; Keller, S. *Nat. Protoc.* **2010**, *5*, 267−281.
(27) Nozaki, Y. *Methods Enzymol.* **1972**, *26* (Pt C), 43−50.
(28) Schleucher, J.; Schwendinger, M.; Sattler, M.; Schmidt, P.; Schedletzky, O.; Glaser, S. J.; Sorensen, O. W.; Griesinger, C. *J. Biomol. NMR* **1994**, *4*, 301−306.
(29) Morris, G. M.; Goodsell, D. S.; Halliday, R. S.; Huey, R.; Hart, W. E.; Belew, R. K.; Olson, A. J. *J. Comput. Chem.* **1998**, *19*, 1639−1662.
(30) Getzoff, E. D.; Gutwin, K. N.; Genick, U. K. *Nat. Struct. Biol.* **2003**, *10*, 663−668.
(31) Ramachandran, P. L.; Lovett, J. E.; Carl, P. J.; Cammarata, M.; Lee, J. H.; Jung, Y. O.; Ihee, H.; Timmel, C. R.; van Thor, J. J. *J. Am. Chem. Soc.* **2011**, *133*, 9395−9404.
(32) Kandori, H.; Iwata, T.; Hendriks, J.; Maeda, A.; Hellingwerf, K. J. *Biochemistry* **2000**, *39*, 7902−7909.
(33) van der Horst, M. A.; van Stokkum, I. H.; Crielaard, W.; Hellingwerf, K. J. *FEBS Lett.* **2001**, *497*, 26−30.
(34) Hendriks, J.; Hoff, W. D.; Crielaard, W.; Hellingwerf, K. J. *J. Biol. Chem.* **1999**, *274*, 17655−17660.
(35) Scholtz, J. M.; Grimsley, G. R.; Pace, C. N. Solvent Denaturation of Proteins and Interpretations of the M Value. *Methods in Enzymology, Vol 466: Biothermodynamics, Pt B*; Elsevier Academic Press Inc: San Diego, CA, 2009; Vol. *466*, pp 549−565.

(36) Rubinstenn, G.; Vuister, G. W.; Mulder, F. A.; Dux, P. E.; Boelens, R.; Hellingwerf, K. J.; Kaptein, R. *Nat. Struct. Biol.* **1998**, *5*, 568−570.
(37) Henzler-Wildman, K.; Kern, D. *Nature* **2007**, *450*, 964−972.
(38) Lindorff-Larsen, K.; Best, R. B.; DePristo, M. A.; Dobson, C. M.; Vendruscolo, M. *Nature* **2005**, *433*, 128−132.
(39) Oktaviani, N. A.; Pool, T. J.; Kamikubo, H.; Slager, J.; Scheek, R. M.; Kataoka, M.; Mulder, F. A. A. *Biophys. J.* **2012**, *102*, 579−586.
(40) Devanathan, S.; Genick, U. K.; Canestrelli, I. L.; Meyer, T. E.; Cusanovich, M. A.; Getzoff, E. D.; Tollin, G. *Biochemistry* **1998**, *37*, 11563−11568.
(41) Kumauchi, M.; Hamada, N.; Sasaki, J.; Tokunaga, F. *J. Biochem.* **2002**, *132*, 205−210.
(42) Borucki, B.; Otto, H.; Joshi, C. P.; Gasperi, C.; Cusanovich, M. A.; Devanathan, S.; Tollin, G.; Heyn, M. P. *Biochemistry* **2003**, *42*, 8780−8790.